Investigation of the Structure and Properties of the Fe-Ni-Co-Cu-V Multiprincipal Element Alloys

A.I. BAZLOV, A.YU. CHURYUMOV, and D.V. LOUZGUINE-LUZGIN

The effect of V addition to the Fe-Ni-Co-Cu system was analyzed in the present work. Three distinct alloys were prepared in a vacuum electric arc furnace in an argon atmosphere and later cast into a copper mold. Investigation of the structure of alloys was performed by scanning electron microscopy (SEM) and by X-ray diffraction. The mechanical properties were also tested in compression. The phase diagrams of the Fe-Ni-Co-Cu-V system were thermodynamically calculated and the results are compared with those of differential scanning calorimetry and the results of SEM observation. It is shown that as a result of crystallization, two solid solutions with FCC crystal structures are formed. The addition of equiatomic amount of vanadium to Fe-Ni-Co-Cu system alloys facilitates phase separation in the liquid state. The addition of V causes an increase in the yield strength by solid solution hardening by about 30 pct and maximum true stress by 40 pct, yet retaining good plasticity. It also does not cause formation of an intermetallic compound.

https://doi.org/10.1007/s11661-018-4871-1

I. INTRODUCTION

FOR many years, numerous experimental and theoretical studies conducted by scientists provided increase in mechanical properties using classical methods: solution hardening, quenching, aging, plastic deformation, etc. However, fundamentally new methods are needed to create a modern class of structural and functional materials. High-strength and ductile materials with high-performance characteristics can be created by using multicomponent compositions without a basic chemical element.[1,2] The main idea of creating multi-principle element alloys (MPEA) without a base component, also called high-entropy alloys (HEA) (though the entropy of solid solutions should be treated with a precaution[3]), is the maximization of entropy in the alloys of multicomponent solid solutions of equimolar or near equimolar composition.[1,2] This is different from the traditional alloys designing approach, which are usually based on one or two basic components. The unique properties of highly alloyed compositions make it possible to use them in different areas, such as tools, die molds, mechanical parts, and furnace parts that require high strength, thermal stability and, at the same time, wear resistance and oxidation resistance at elevated temperatures.[4–6] Most of the research works so far was focused on the Fe-Ni alloys containing Co, Cr, Cu, Al, Ti, or Mn.[7–12] Refractory metals alloys of MPEA type were also successfully created[13,14] and some of those were low-density alloys.[15,16] There are also attempts to create light metal MPEAs.[17] The atomic structure of the MPEAs was studied in detail.[18] The MPEAs are found to be good as corrosion-resistant alloys in various aqueous environments.[19]

However, the vast majority of alloys with several base elements contain several phases, whereas only carefully selected alloy compositions can form single-phase solid solution structures.[4,20] Arbitrary mixing of the elements from the periodic table often leads to the formation of multiphase structures, rather than a single-phase solid solution. For example, Cantor *et al.*[21] investigated 20- and 16-component alloys with equimolar atomic ratios and several crystalline phases were found to form. They were brittle both in the form of cast ingots and melt-spun ribbons. Although it was possible to produce a single FCC-phase Co-Cr-Fe-Mn-Ni alloy, the attempts to incorporate additional elements into the solid solution (in equiatomic quantities) failed. In Reference 22, five-component alloys based on the Co-Cr-Fe-Mn-Ni system were studied by replacing one element at a time using a chemically similar element, but again all new alloys consisted of more than one phase in the cast state. These experiments showed that the configurational entropy does not always play a dominant role in determining the phase stability versus enthalpy and, consequently, in the microstructure of the alloy.[22] The scanning electron microscope elemental

A.I. BAZLOV and A. YU. CHURYUMOV are with the National University of Science and Technology 'MISiS', Moscow, Russia 119049. Contact e-mail: churyumov@misis.ru D.V. LOUZGUINE-LUZGIN is with the WPI Advanced Institute for Materials Research, Tohoku University, Sendai 980-8577, Japan.

Manuscript submitted March 29, 2018.
Article published online August 23, 2018

maps obtained within the as-solidified dendrites in a chill cast single-phase FCC 5-component $Cr_{20}Mn_{20}Fe_{20}Co_{20}Ni_{20}$ alloy, in addition showed that Cr and Fe segregated into the dendrite spines and Mn segregated into the interdendritic spaces. The as-solidified dendrites in a more complex chill cast 7-component $Cr_{14.3}Mn_{14.3}Fe_{14.3}Co_{14.3}Ni_{14.3}V_{14.3}Ti_{14.3}$ alloy, with Cr and Mn segregated in the dendrite spines and V and Ti segregated into the interdendritic spaces.[21]

The MPEA/HEA alloys are usually strengthened by the addition of Al or Ti. Al addition promotes the formation of a BCC phase. Co-Cr-Fe-Ni-Ti-Al system alloys with different Al contents were homogenized at 1273 K for 2 hours. Annealing showed no obvious influence on the phase composition and elemental segregation of Co-Cr-Fe-Ni-Ti-Al alloys.[23]

The establishment of universal rules for the formation of HEA is not trivial, due to a number of empirical parameters, including the difference in atomic sizes, enthalpy, and other factors. Despite the usefulness of these empirical rules, they may not be able to convincingly explain the experimental facts. In fact, the most intuitive and rational way to estimate phase stability in MPEA alloys is to analyze them using phase diagrams, as noted in References 24 and 25, and also in References 26 and 27. As a rule, phase diagrams are constructed based on the experimental data of equilibrium states obtained from the results of thermal and structural analyses, which are usually labor-intensive and expensive, especially for multicomponent systems. Application of thermodynamic modeling of multicomponent systems using the CALPHAD method (abbreviation of CALculation of PHAse Diagrams) allows reducing significantly time and material costs.[28] The CALPHAD method combines experimental data on phase equilibria of systems and all thermodynamic information, which makes it possible to calculate thermodynamic properties for multicomponent systems without additional experiments.[25]

Influence of V addition on the microstructure and mechanical properties of the Al0.5CoCrCuFeNi alloy was studied and it was found that V stabilizes BCC phase and drastically increases the alloy hardness.[29] σ phase was found to form in a certain composition range. Effect of V and Mn additions on the structure and mechanical properties of the equiatomic CoCrFeNiV and CoCrFeNiMnV alloys was also studied earlier.[30] As could be expected from the phase diagrams, a tetragonal lattice-type σ phase was formed in the CoCrFeNiV and CoCrFeNiMnV alloys[22,30] leading to drastic embrittlement of the samples.

Vanadium is a neighbor element of Ti in the periodic table (which is routinely used to strengthen the MPEAs) but located closer to the late transition metals (LTMs). Although being an early transition metal as Ti, V nevertheless has a closer atomic size to LTMs[31] compared to Ti and, according to the phase diagrams, exhibits less tendency for the formation of intermetallic compounds with LTMs. According to Reference 32, V can induce the formation of second solid solution phase. Thus, in the present work, we study the effect of V addition on the structure and properties of the Fe-Ni-Co-Cu system alloys. Based on our preliminary studies, we deliberately excluded Cr from this alloy because it can cause the formation of the ordered σ phase with Fe and embrittle the samples. It was substituted with Cu, which, however, can trigger phase separation in the studied alloys.[33] Also as V is rather an early transition metal, its concentration should be preferably lower than that of late transition metals in order to avoid possible formation of an ordered compound with Fe, Ni, or Co.

II. EXPERIMENTAL PROCEDURE

Chemical compositions of the studied alloys are shown in Table I. The preparation of alloys was carried out from pure elements (> 99.9 wt pct purity) in a vacuum electric arc furnace on a copper water-cooled hearth. Melting was carried out in an argon atmosphere with Ti as a getter. The obtained ingots were turned over and re-melted for four times. After four times of re-melting, the received ingots were uniform in chemical composition. The cast samples were produced by casting into a copper mold.[34] Investigation of the structure of alloys was performed by scanning electron microscopy (SEM) in a microscope equipped with energy-dispersive X-ray analysis and by X-ray diffraction. In order to determine the mechanical properties of alloys, compression tests were carried out on cylindrical specimens, 7.5 mm in height and 5 mm in diameter. The strain rate was 10^{-2} s^{-1}. The compression tests were performed using graphite powder as a lubricant. Thermal properties of the samples were performed by differential scanning calorimetry (DSC) at the heating and cooling rate of 0.33 K/s. Thermodynamic calculations of the phase diagrams were performed using the Thermocalc software with the iron-based alloys thermodynamic database TCFe7. The database includes all 10 binary systems and 6 ternary systems, Fe-Co-V, Fe-Cu-V, Fe-Co-Ni, Fe-Cu-Ni, Fe-Ni-V, Fe-Co-Cu, related to the studied alloy system. The composition limitations for this

Table I. Chemical Compositions and Characteristic Temperatures of the Studied Alloys Obtained by Thermodynamic Modeling Using the Thermocalc Software Together with the Approximate Experimental Values

Alloy	Composition	T_s^c (K)	T_l^c (K)	T_s^{e*} (K)	T_l^{e*} (K)	ΔT_s
	$Fe_{25}Ni_{25}Co_{25}Cu_{25}$	1610	1647	—	—	37
V-5	$Fe_{23.75}Ni_{23.75}Co_{23.75}Cu_{23.75}V_5$	1551	1609	1421	> 1673	> 252
V-10	$Fe_{22.5}Ni_{22.5}Co_{22.5}Cu_{22.5}V_{10}$	1475	1589	1409	> 1673	> 264
V-20	$Fe_{20}Ni_{20}Co_{20}Cu_{20}V_{20}$	1444	1512	1391	1612	221

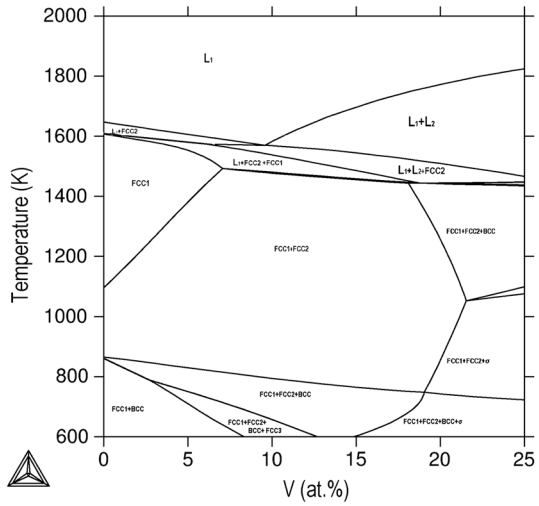

Fig. 1—The polythermal section of the calculated phase diagram (FeNiCoCu)–V.

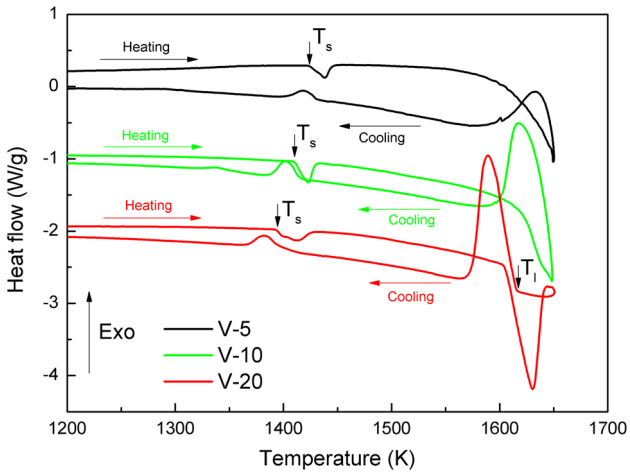

Fig. 2—The DSC curves of the investigated alloys.

database are maximum 19 at. pct Co, maximum 4.5 at. pct Cu, maximum 19 at. pct Ni, maximum 16 wt. pct V, and minimum 50 at. pct Fe.

III. RESULTS

When vanadium is added substituting for all four base components, at 6 at. pct V and at more than 1470 K, phase separation occurs in the liquid state, and at a certain V content the intermetallic phase σ appears (Figure 1). It can also be noted that although with the addition of vanadium, the calculated liquidus T_l^c and solidus T_s^c temperature are reduced, the crystallization interval of the alloys expands to about 120 K at 7 at. pct V and then slightly narrows to 100 K at 20 at. pct V. The $Fe_{23.75}Ni_{23.75}Co_{23.75}Cu_{23.75}V_5$ alloy (Figure 1) has the solidus temperature of 1551 K and the liquidus temperature is 1609 K. The alloy with 10 at. pct V is characterized by a broad crystallization interval with the solidus and liquidus temperatures of 1475 K and 1589 K, respectively. The intermetallic σ phase is present at low temperature. Phase separation occurs in the $Fe_{20}Ni_{20}Co_{20}Cu_{20}V_{20}$ alloy in the liquid state at high temperature. σ phase appears to form below 859 K. The solidus temperature reaches 1444 K, and the liquidus temperature reaches 1512 K. The resulted data are shown in Table I.

The DSC curves are presented at Figure 2 and the resulted approximate experimental solidus T_s^{e*} and liquidus T_l^{e*} temperature values are also summarized in Table I. As one can see in Figure 2, the first endothermic peak on the heating curve has a slightly asymmetrical shape. Its first (left) shoulder corresponds to melting of the FCC2 phase. The FCC2 phase has a lower solidus temperature due to higher copper concentration. The addition of vanadium reduces the solidus temperature of the alloys much more than the liquidus, thereby increasing the crystallization interval. An increase in the crystallization interval is not desirable, because excessive shrinkage porosity may occur during

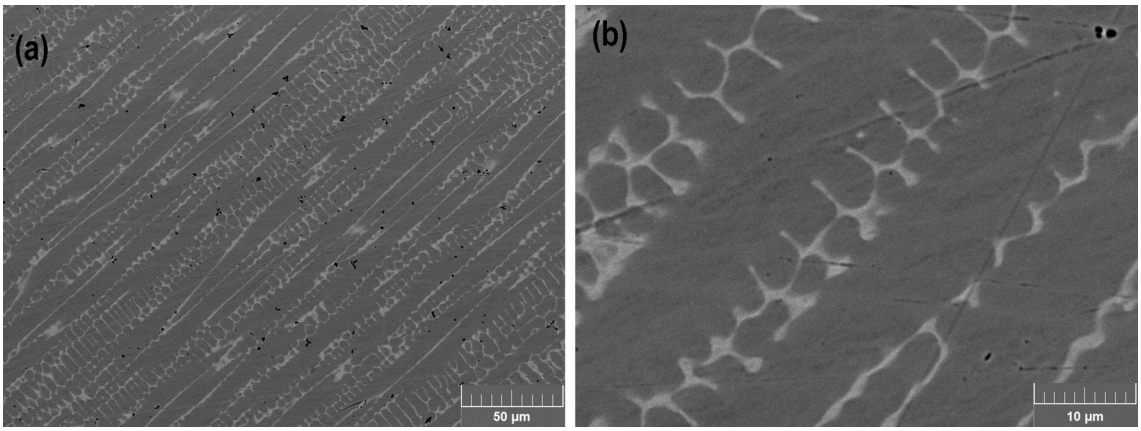

Fig. 3—Microstructure of V-5 alloy at low (*a*) and high (*b*) magnification.

casting, which in turn will lead to cracking during further mechanical treatment.

Figures 3 and 4 show the SEM microstructure, and the XRD pattern of the V-5 alloy. Chemical composition of the existing phases is shown in Table II. The FCC2 (light phase) is strongly enriched in copper and depleted in all other elements according to the most of binary phase diagrams[33] representing low solubility of Cu in other constituent elements except for the Cu-Ni one in which phase separation occurs at low temperature. The structure of the V-5 alloy in the cast state is a solid solution FCC1 with an FCC lattice and a degenerate eutectic crystallized in the interdendritic space, forming a second phase also having an FCC lattice. The lattice parameters of these two phases are very close to each other. In this connection, it is very hard to distinguish them in the XRD pattern—the peaks are superimposed on each other and only high-angle peaks have some shoulders as shown in the inset in Figure 4. The approximate values of the lattice parameters are also given. Crystallization porosity associated with a wide range of crystallization of the alloy is observed in Figure 3.

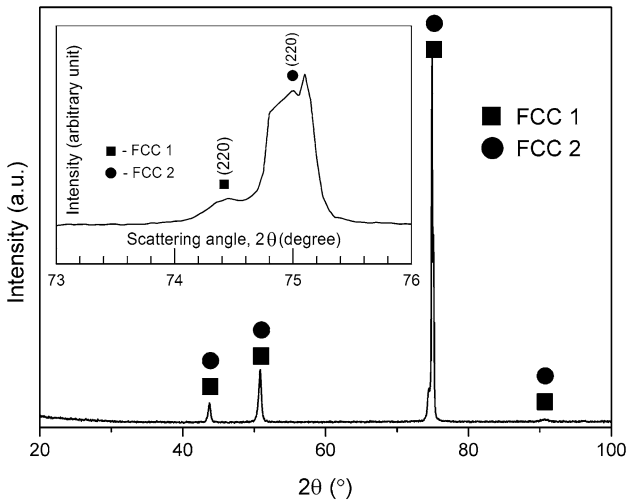

Fig. 4—X-ray diffraction pattern of the V-5 alloy. The inset shows a close-up of (220) peaks.

SEM micrographs and the XRD pattern of the V-10 alloy are presented in Figures 5 and 6. The structure of the V-10 alloy in the cast state is a solid solution with FCC lattice and a degenerate eutectic crystallized in the interdendritic space. The second phase also has a FCC lattice. Similar to V-5, the lattice parameters of these two phases are very close to each other and only high-angle peaks have some shoulders. Porosity of crystallization origin associated with a wide crystallization range of the alloy can also be observed in Figure 5. Table III shows the EDX analysis results of the V-10 alloy together with the approximate values of the lattice parameters. Again the FCC2 (light phase) is strongly enriched in copper and depleted in all other elements.

Figures 7 and 8 show the SEM micrographs and the XRD pattern of the V-20 alloy. The structure is a mixture of two solid solutions and the second one is based on copper. Such a structure is the result of phase separation in the liquid state which results from the addition of a large amount of vanadium to the alloy. Also, there is a large fraction of pores and vanadium oxides in the structure, which could have a negative

Table II. Lattice Parameters and Chemical Composition of Two Phases in the V-5 Alloy

Phase	*a*, pm	Atomic Percent				
		V	Fe	Co	Ni	Cu
Dark Color (Dendritic) Phase, FCC1	359	5.3 ± 0.6	27.5 ± 2.2	27.9 ± 2.0	24.4 ± 1.8	14.9 ± 1.6
Light Color (Interdendritic) Phase, FCC2	358	1.3 ± 0.1	9.3 ± 0.8	9.1 ± 0.5	11.4 ± 0.5	68.9 ± 5.7

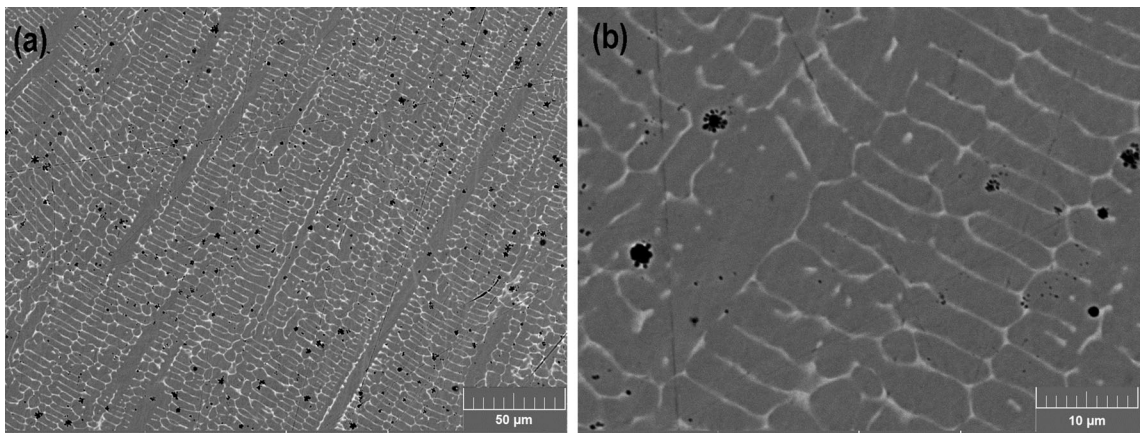

Fig. 5—Microstructure of V-10 alloy at low (*a*) and high (*b*) magnification.

effect on the technological properties of the alloy. Oxygen as light element scatters X-rays much less efficiently than metals and the patterns of oxides are absent on the XRD pattern in Figure 8. In many alloys, oxides have a faceted needle- or plate-like morphology and act as stress concentrators thus reducing plasticity. However, in the V-bearing alloys, in particular in V-20, the V-rich oxide phase has a rounded flower-type morphology (see Figure 7) which is not a stress concentrator and does not deteriorate the mechanical properties.

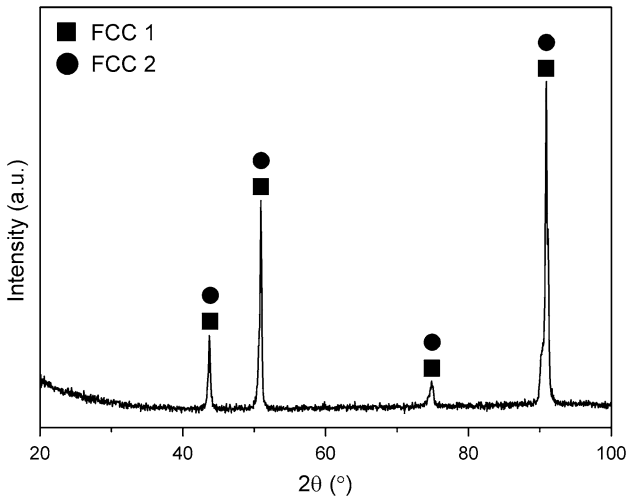

Fig. 6—X-ray diffraction pattern of the V-10 alloy.

Rather surprisingly, no σ phase was formed in this alloy. Thus, one could suggest that σ phase formed in the CoCrFeNiV alloy[30] is a result of joint alloying with Cr and V and it was right decision to exclude Cr from the alloy composition. Table IV shows the results of EDX analysis for the V-20 alloy together with the approximate values of the lattice parameters.

Figure 9 shows the compression mechanical test curves of the investigated alloys. After reaching a deformation of 50 pct of engineering strain, the tests were stopped. It is seen from the presented graphs that these alloys having a solid solution structure with nonequilibrium eutectic have rather low values of yield strength (from 300 to 500 MPa), but it is drastically hardened during deformation and their strength exceeds 1000 MPa. The deformation of these alloys proceeds without any fracture at least until 47 pct of engineering strain. It should be noted that an increase in the concentration of vanadium favorably affects the mechanical properties of alloys: it increases the yield strength and ultimate strength, while retaining large plastic deformation.

Table V shows the mechanical properties of the investigated alloys in the as-cast state and reference data for the $Fe_{25}Ni_{25}Co_{25}Cu_{25}$ one.[35]

Table III. Lattice Parameters and Chemical Composition of Two Phases in the V-10 Alloy

Phase	*a*, pm	Atomic Percent				
		V	Fe	Co	Ni	Cu
Dark Color (Dendritic) Phase, FCC1	360	10.7 ± 1.1	25.6 ± 2.8	26.0 ± 2.3	23.6 ± 2.7	14.1 ± 1.5
Light Color (Interdendritic) Phase, FCC2	359	3.6 ± 0.4	10.3 ± 0.5	9.5 ± 1.0	13.2 ± 1.4	63.4 ± 5.1

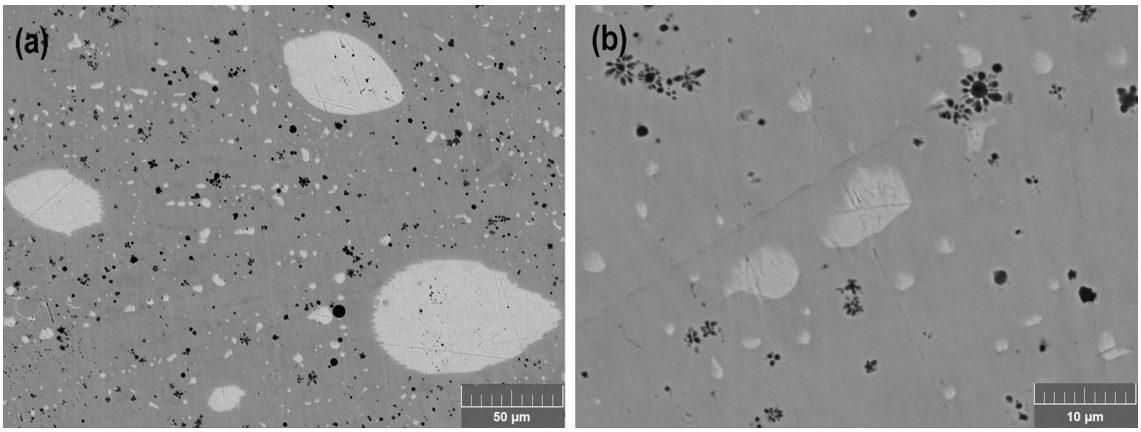

Fig. 7—Microstructure of V-20 alloy at low (*a*) and high (*b*) magnification.

IV. DISCUSSION

The CALPHAD calculations rightfully indicate that 1) two solid solutions are expected to form in the studied alloys and 2) phase separation takes place even in the liquid state at certain compositions. On the other hand, as can be seen from the comparison of the calculated and experimental values of the solidus and liquidus temperatures of the investigated alloys, a discrepancy is observed. The discrepancy between the liquidus and solidus temperatures of the alloys can be explained by insufficient thermodynamic data in the database. The calculation was made using the parameters of binary and ternary phase diagrams available up to date, and for a more accurate calculation, it is necessary to obtain and optimize the databases for the multicomponent systems. Similarly, the differences in the solidus temperatures can be explained by the presence in the alloys of nonequilibrium low-melting phases formed during nonequilibrium crystallization.

It was found that in the $Fe_{25}Ni_{25}Co_{25}Cu_{25}$ alloy, the dendrites are enriched in Fe and Co, while interdendritic region is enriched in Cu and distribution of Ni is more uniform.[35] Similar results are obtained in the present work but according to thermodynamic calculations, the interdendritic regions represent not a dendritic liquation but another minor FCC phase different in composition (enriched in Cu).

Although, the chemical composition of the phases is different owing to very similar atomic size of the consisting LTMs, the diffraction peaks superimpose and the X-ray diffraction patterns look like those of a single-phase material. Although V has atomic size different from the other elements by about 6 pct,[31] its concentration does not exceed 20 at. pct and this element is present in both FCC phases. Such a difference caused broadening of the X-ray diffraction peaks but allowed approximate determination of the lattice parameters of two FCC phases which are very close to each other. As expected they increased with an increase in V content.

Opposite to earlier results[29,30] and expectations from the calculated equilibrium phase diagrams, no σ phase was found in the studied alloys. It likely happens owing to the absence of Cr which is another σ phase forming element in such alloys and a nonequilibrium structure formed on solidification in Cu mold of 5 mm diameter in which the cooling rate of metallic alloys at high temperature reaches hundreds of Kelvin per second.[34] The V-20 alloy contains a large fraction of the oxide particles likely owing to high chemical reactivity of V with oxygen.

Although, the studied alloys have rather low values of yield strength (ranged from 300 to 500 MPa) they are strongly hardened during deformation and the ultimate true strength of V-20 alloy exceeds 1000 MPa with at least 47 pct of engineering strain. Thus, an increase in the vanadium content improves the mechanical properties of alloys without deterioration of plasticity, in particular, owing to rounded morphology of the oxide phase in V-20 alloy. The addition of V causes an increase in the yield and ultimate strength by solid solution hardening and even at 20 at. pct of V content

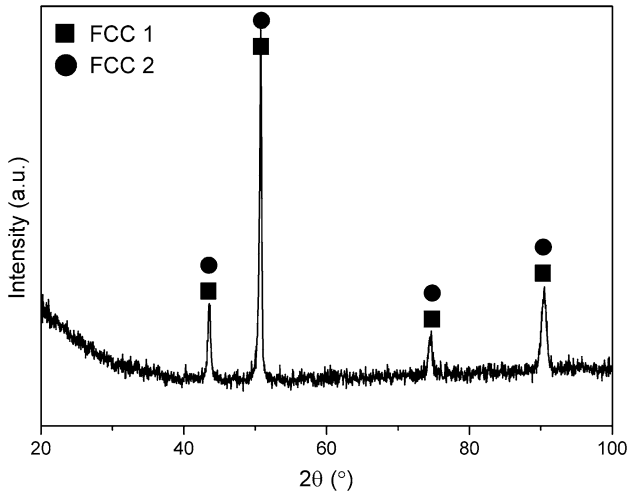

Fig. 8—X-ray diffraction pattern of the V-20 alloy.

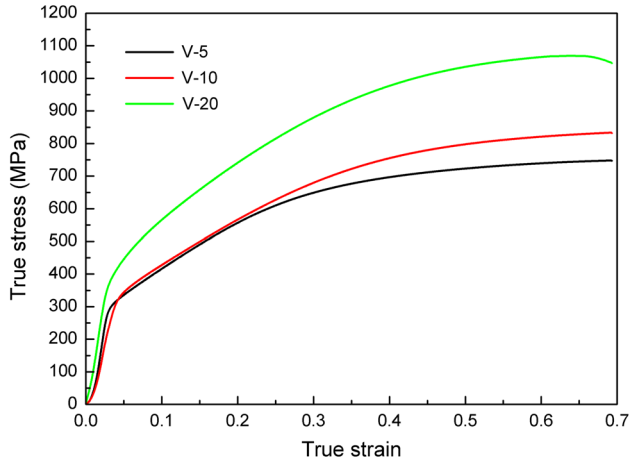

Fig. 9—Stress–strain curves of the studied alloys.

Table IV. Lattice Parameters and Chemical Composition of the Thermodynamic Phases in the V-20 Alloy

		Atomic Percent					
Phase	*a*, pm	O	V	Fe	Co	Ni	Cu
Dark Color (Dendritic) Phase, FCC1	362	—	20.2 ± 1.2	22.8 ± 2.7	23.5 ± 2.4	21.4 ± 2.6	12.1 ± 0.6
Light Color (Interdendritic) Phase, FCC2	360	—	0.7 ± 0.1	3.6 ± 0.4	2.7 ± 0.3	6.5 ± 0.8	86.5 ± 7.8
Oxide Phase	—	34.3 ± 2.7	41.8 ± 3.2	4.3 ± 0.5	4.1 ± 0.6	3.6 ± 0.5	11.9 ± 1.4

Table V. Mechanical Properties of Studied Alloys and the Base One

Alloy	Yield Strength (MPa)	Ultimate True Strength (MPa)	True Strain
$Fe_{25}Ni_{25}Co_{25}Cu_{25}$	~ 290	~ 480*	~ 0.12*
V-5	304 ± 21	~ 750	> 0.65
V-10	295 ± 16	~ 830	> 0.65
V-20	370 ± 27	~ 1070	> 0.65

* in tension.

do not cause formation of the intermetallic compounds though oxidation takes place at high V content owing to high reactivity of this element.

V. CONCLUSIONS

The phase diagrams of the Fe-Ni-Co-Cu-V system were thermodynamically calculated using TCFE7 database and qualitatively corresponded to those measured by differential scanning calorimetry though the resulted characteristic temperatures are somewhat different. It is found that two solid solutions with FCC lattice are formed on crystallization. The addition of more than 10 pct of vanadium to Fe-Ni-Co-Cu system alloys facilitates phase separation even in the liquid state and formation of the globular inclusions of Cu-rich phase. The addition of V causes an increase in the yield and maximum strength by solid solution hardening and even at 20 at. pct of V content it does not cause formation of the intermetallic compounds. The addition of vanadium improves the mechanical properties without deterioration of plasticity, in particular, owing to rounded morphology of the oxide phase in V-20 alloy.

ACKNOWLEDGMENTS

The authors gratefully acknowledge the financial support received from the Ministry of Education and Science of the Russian Federation in the framework of the "Increase Competitiveness" Program of NUST "MISiS" (No. K2-2014-013 and K2-2017-089).

REFERENCES

1. J.W. Yeh, S.K. Chen, S.J. Lin, J.Y. Gan, T.S. Chin, T.T. Shun, C.H. Tsau, and S.Y. Chang: *Adv. Eng. Mater.*, 2004, vol. 6, pp. 299–303.
2. B. Cantor: *Entropy*, 2014, vol. 16 (9), pp. 4749–68.
3. I.A. Tomilin and S.D. Kaloshkin: *Mater. Sci. and Tech.*, 2015, vol. 31, pp. 1231–34.
4. D.B. Miracle and O.N. Senkov: *Acta Mater.*, 2017, vol. 122, pp. 448–511.
5. E. Fazakas, V. Zadorozhnyy, and D.V. Louzguine-Luzgin: *Appl. Surf. Sci.*, 2015, vol. 358, pp. 549–55.
6. K.Y. Tsai, M.H. Tsai, and J.W. Yeh: *Acta Mater.*, 2013, vol. 61, pp. 4887–97.
7. Y.J. Zhou, Y. Zhang, Y.L. Wang and G.L. Chen: Appl. Phys. Lett., 2007, V. 90, pp. 181904 (1-3).
8. S.T. Chen, W.Y. Tang, Y.F. Kuo, S.Y. Chen, C.H. Tasu, T.T. Shun, and J.W. Yeh: *Mater. Sci. Eng. A*, 2010, vol. 527, pp. 5818–25.
9. W.R. Wang, W.L. Wang, S.C. Wang, Y.C. Tsai, C.H. Lai, and J.W. Yeh: *Intermetallics*, 2012, vol. 26, pp. 44–51.
10. J.Y. He, W.H. Liu, H. Wang, Y. Wu, X.J. Liu, T.G. Nieh, and Z.P. Lu: *Acta Mater.*, 2014, vol. 62, pp. 105–13.
11. J.W. Yeh, S.J. Lin, T.S. Chin, J.Y. Gan, S.K. Chen, T.T. Shun, C.H. Tsau, and S.Y. Chou: *Metall. Mater. Trans. A*, 2004, vol. 35A, pp. 2533–36.
12. Y. Zhang, S.G. Ma, and J.W. Qiao: *Metall. Mater. Trans. A*, 2012, vol. 43A, pp. 2625–30.
13. O.N. Senkov, G.B. Wilks, D.B. Miracle, C.P. Chuang, and P.K. Liaw: *Intermetallics*, 2010, vol. 18, pp. 1758–65.
14. E. Fazakas, V. Zadorozhnyy, L. Varga, A. Inoue, D.V. Louzguine-Luzgin, F. Tian, and L. Vitos: *Int. J. Refract. Met. Hard Mater.*, 2014, vol. 47, pp. 131–38.
15. O. Senkov, S. Senkova, C. Woodward, and D. Miracle: *Acta Mater.*, 2013, vol. 61, pp. 1545–57.
16. N. Stepanov, N.Y. Yurchenko, D. Shaysultanov, G. Salishchev, and M. Tikhonovsky: *Mater. Sci. Technol.*, 2015, vol. 31, pp. 1184–93.
17. K.M. Youssef, A.J. Zaddach, C. Niu, D.L. Irving, and C.C. Koch: *Mater. Res. Lett.*, 2015, vol. 3, pp. 95–99.
18. H. Diao, L.J. Santodonato, Z. Tang, T. Egami, and P.K. Liaw: *JOM*, 2015, vol. 67, pp. 2321–25.
19. Y.Z. Shi, B. Yang and P. K. Liaw: Metals, 2017, V. 7(2), 43.
20. M.C. Troparevsky, J.R. Morris, M. Daene, Y. Wang, A.R. Lupini, and G.M. Stocks: *JOM*, 2015, vol. 67, pp. 2350–63.
21. B. Cantor, I.T.H. Chang, P. Knight, and A.J.B. Vincent: *Mater. Sci. Eng. A*, 2004, vols. 375–377, pp. 213–18.
22. F. Otto, Y. Yang, H. Bei and E.P. George: *Acta Mater.*, 2013, vol. 61, pp. 2628–38.
23. K.B. Zhang and Z.Y. Fu: *Intermetallics*, 2012, vol. 22, pp. 24–32.
24. C. Zhang, F. Zhang, S. Chen, and W. Cao: *JOM*, 2012, vol. 64 (7), pp. 839–45.
25. F. Zhang, C. Zhang, S. Chen, J. Zhu, W. Cao, and U.R. Kattner: *CALPHAD*, 2014, vol. 45, pp. 1–10.
26. M.C. Gao and D.E. Alman: *Entropy*, 2013, vol. 15, pp. 4504–19.
27. R. Feng, M.C. Gao, C. Lee, M. Mathes, T. Zuo, S. Chen, J.A. Hawk, Y. Zhang and P.K. Liaw: *Entropy*, 2016, vol. 18, pp. 333 (1–21).
28. M.C. Gao, B. Zhang, S. Yang, and M. Guo: *Metall. Mater. Trans. A*, 2016, vol. 47A, pp. 3333–39.
29. M.-R. Chen, S.-J. Lin, J.-W. Yeh, M.-H. Chuang, S.-K. Chen, and Y.-S. Huang: *Metall. Mater. Trans. A*, 2006, vol. 37A, pp. 1363–69.
30. G.A. Salishchev, M.A. Tikhonovsky, D.G. Shaysultanov, N.D. Stepanov, A.V. Kuznetsov, I.V. Kolodiy, A.S. Tortika, and O.N. Senkov: *J. Alloys Compd.*, 2014, vol. 591, pp. 11–21.
31. M.A. Burlington:Smithells Metals Reference Book. 8th ed in *ASM International Metals Reference Book*, W.F. Gale and T.C. Totemeier, eds., Elsevier Butterworth-Heinemann Ltd., Oxford UK, 2004, pp. 4–44.
32. M.C. Troparevsky, J.R. Morris, P.R.C. Kent, A.R. Lupini, and G.M. Stocks: *Phys. Rev. X*, 2015, vol. 5, p. 011041.
33. M.A. Burlington:Smithells Metals Reference Book. 8th ed in *ASM International Metals Reference Book*, W.F. Gale and T.C. Totemeier, eds., Elsevier Butterworth-Heinemann Ltd., Oxford UK, 2004, pp. 11–11.
34. D.V. Louzguine-Luzgin, T. Saito, J. Saida, and A. Inoue: *J. Mater. Res.*, 2008, vol. 23, pp. 515–22.
35. L. Liu, J.B. Zhu, C. Zhang, J.C. Liu, and Q. Jiang: *Mater. Sci. Eng. A*, 2012, vol. 548, pp. 64–68.